SCIENTIFIC REPORTS
nature research

OPEN

Single Source Thermal Evaporation of Two-dimensional Perovskite Thin Films for Photovoltaic Applications

Zhuang-Hao Zheng[1], Hua-Bin Lan[2], Zheng-Hua Su[1], Huan-Xin Peng[1], Jing-Ting Luo[1], Guang-Xing Liang[1*] & Ping Fan[1]

Hybrid two-dimensional (2D) halide perovskites has been widely studied due to its potential application for high performance perovskite solar cells. Understanding the relationship between microstructural and opto-electronic properties is very important for fabricating high-performance 2D perovskite solar cell. In this work, the effect of solvent annealing on grain growth was investigated to enhance the efficiency of photovoltaic devices with 2D perovskite films based on $(BA)_2(MA)_3Pb_4I_{13}$ prepared by single-source thermal evaporation. Results show that solvent annealing with the introduction of solvent vapor can effectively enhance the crystallization of the $(BA)_2(MA)_3Pb_4I_{13}$ thin films and produce denser, larger-crystal grains. The thin films also display a favorable band gap of 1.896 eV, which benefits for increasing the charge-diffusion lengths. The solvent-annealed $(BA)_2(MA)_3Pb_4I_{13}$ thin-film solar cell prepared by single-source thermal evaporation shows an efficiency range of 2.54–4.67%. Thus, the proposed method can be used to prepare efficient large-area 2D perovskite solar cells.

Solar energy is a green clean energy source with a wide range of applications. Organic–inorganic hybrid perovskite solar cells have drawn great attention thanks to their high photoelectric conversion efficiency, simple manufacturing, and low cost[1–3]. The initial efficiency of perovskite solar cells was only 3.8%, but recently, the efficiency of single-junction perovskite solar cells has reached a high record to 24.2%[4] and the perovskite/silicon tandem solar cell incresed to 25.2%[5].

The device structures, recombination mechanisms, interface engineering, and material synthesis should be studied to further improve the efficiency. The key to improving the efficiency of solar cells is to improve the quality of perovskite film[6]. Solvent annealing is reportedly as an effective way to improve the crystallinity of some organic semiconductors, but this method's effectiveness in inorganic semiconductors has not yet been confirmed. The current study shows that solvent annealing can be applied to increase the crystallinity and grain size of the perovskite films. Huang *et al.* found that the introduction of DMF/DMSO solvent vapor during the growth of $CH_3NH_3PbI_3$ crystals can effectively improve the crystallinity and grain size of the film, passivate the film defects, and improve the device performance[7]. Liu *et al.* reported the introduction an anti-solvent vapor (e.g., alcohol vapor) to replace DMF vapor during the annealing procedure, which can improve the growth of perovskite crystals and increase the grain size of the perovskite $MAPbI_3$ crystals, thus high crystallinity and pinhole-free $MAPbI_3$ film could be obtained[8]. Zhang *et al.* created a different solvent atmosphere to anneal the perovskite film, the results show that the perovskite crystal quality was significantly improved when annealing in a poor mixed solvent [IPA: DMF = 100:1 (v/v)][9].

In addition to efficiency, the environmental stability and light stability under operating conditions are other key factors in photovoltaic and other optoelectronic applications[10]. Compared with its 3D counterpart, the Ruddlesden–Popper phase layered 2D perovskite thin film shows good stability but low efficiency[11,12]. The poor efficiency could be attributed to the inhibition of the out-of-plane charge transport of organic cations, which acted like insulating spacers between conductive inorganic plates[13]. Recently, attempts to utilize two-dimensional layered hybrid compounds in perovskite films have achieved breakthrough results. Smith I.C. *et al.* reported a layered $(PEA)_2(CH_3NH_3)_2Pb_3I_{10}$ perovskite light absorber for solar cell applications. The solar cell has an interesting open circuit voltage of 1.18 V and a photoelectric conversion efficiency of 4.73%. Moreover, this absorber was relatively stable up to 46 days in air with 52% relative humidity[14,15]. Mitzi D.B. explored the photovoltaic-related

[1]Shenzhen Key Laboratory of Advanced Thin Films and Applications, College of Physics and Optoelectronic Engineering, Shenzhen University, Shenzhen, 518060, P.R. China. [2]College of Engineering Physics, Shenzhen Technology University, Shenzhen, 518118, P.R. China. *email: lgx@szu.edu.cn

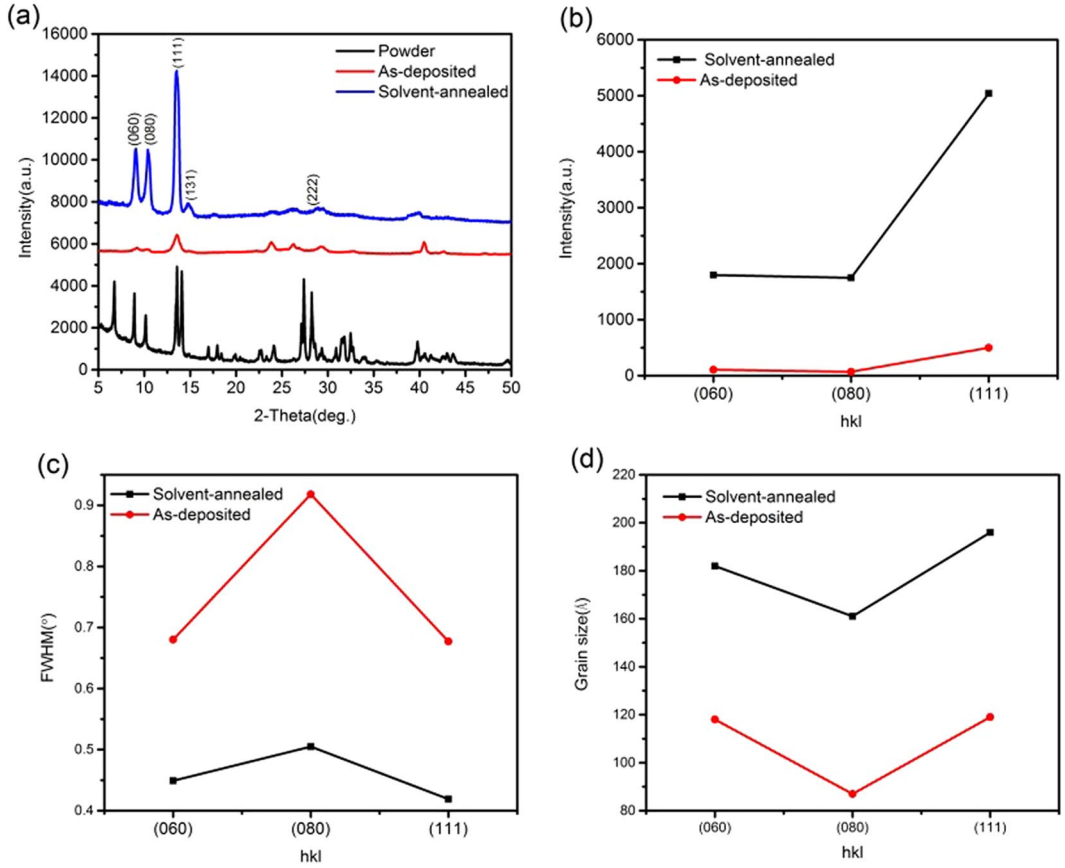

Figure 1. XRD patterns of the (**a**) $(BA)_2(MA)_3Pb_4I_{13}$thin films prepared by single-source thermal evaporation, (**b**) changes in the typical peak intensities, (**c**) FWHM changes, and (**c**) change in grain size.

properties of 2D $MA_2Pb(SCN)_2I_2$ perovskite, which can be used as an absorber layer for the top cell of a tandem solar cell[16]. Although superior device performance has not yet been achieved, this 2D layered mixtures have been demonstrated as effective new perovskite film with adjustable photoelectric properties and enhanced air stability[17,18]. In contrast to 3D perovskite, 2D perovskite $[CH_3(CH_2)_3NH_3)_2(CH_3NH_3)_{n-1}Pb_nI_{3n+1}$ $(BA)_2(MA)_{n-1}Pb_nI_{3n+1}$, $n = 1, 2, 3, 4, \ldots, \infty]$ have better optoelectronic property tunability because of their greater degree of freedom in quantum mechanics and chemistry, and, more importantly, higher environmental stability. Therefore, the development of 2D perovskite thin films will directly aid in improving the stability of perovskite solar cells.

Based on vacuum preparation method, the dual-source or single-source thermal evaporation methods, are also available to deposit perovskite thin films[19–21]. However, the dual-source thermal evaporation requires precise simultaneous control of the evaporation source of organic and inorganic materials, but the effective control of the film compounding process is very difficult. The easy deviation from the stoichiometric ratio directly leads to a decrease in film quality and repeatability[22]. To our knowledge, single-source thermal evaporation is a effective method for preparing large-area, high-efficiency perovskite solar cells[23]. In this study, 2D perovskite $(BA)_2(MA)_3Pb_4I_{13}$ thin film was prepared by single-source thermal evaporation, and the effects of solvent annealing on the microstructural and optoelectronic properties of the thin film were investigated.

Results

Figure 1a shows the crystal structure of the $(BA)_2(MA)_3Pb_4I_{13}$ powder and the thin films including the as-deposited and solvent-annealed thin films. The prepared $(BA)_2(MA)_3Pb_4I_{13}$ powders have characteristic diffraction peaks of 2D perovskite. However, the as-deposited thin film shows broad peaks, which indicates low crystallinity. After the solvent annealing, the stronger characteristic diffraction peaks of the (060), (080), (111), (131), and (222) planes usually refer to the 2D $(BA)_2(MA)_3Pb_4I_{13}$ perovskite crystal structure. These results indicate that the perovskite crystallinity is increased, with fewer low-dimensional defects and/or larger perovskite grain sizes, and less scattering of internal grain boundaries (Fig. 1b)[24–27]. Figure 1c displays the FWHM of the 2D perovskite (060), (080), and (111) peaks. The FWHM of the solvent-annealed thin film is significantly smaller, indicating better crystallization[28]. Based on the Debye-Scherrer formula, $D = K\lambda/(\beta\cos\theta)$, ($D$ is the grain size of crystals, K is a constant, $\lambda$is the wavelength of the X-ray, $\beta$is the FWHM, and θ is the diffraction angle[29]), the grain sizes of the as-prepared and solvent-annealed thin films were calculated and the results are shown in Fig. 1d. After solvent annealing, the 2D perovskite grain size becomes markedly larger, suggesting that the solvent annealing can improve the crystallinity of the thin film, which might lead to a higher efficiency for device.

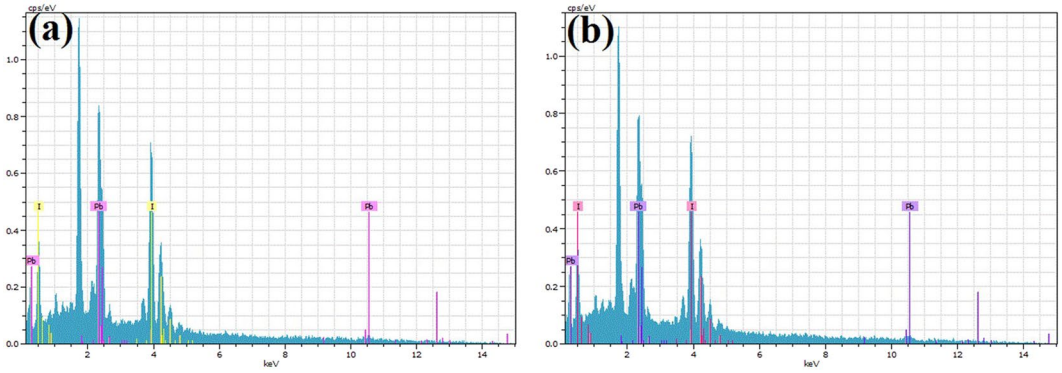

Figure 2. The EDS spectral line patterns of the (**a**) as-deposited and (**b**) solvent-annealed films.

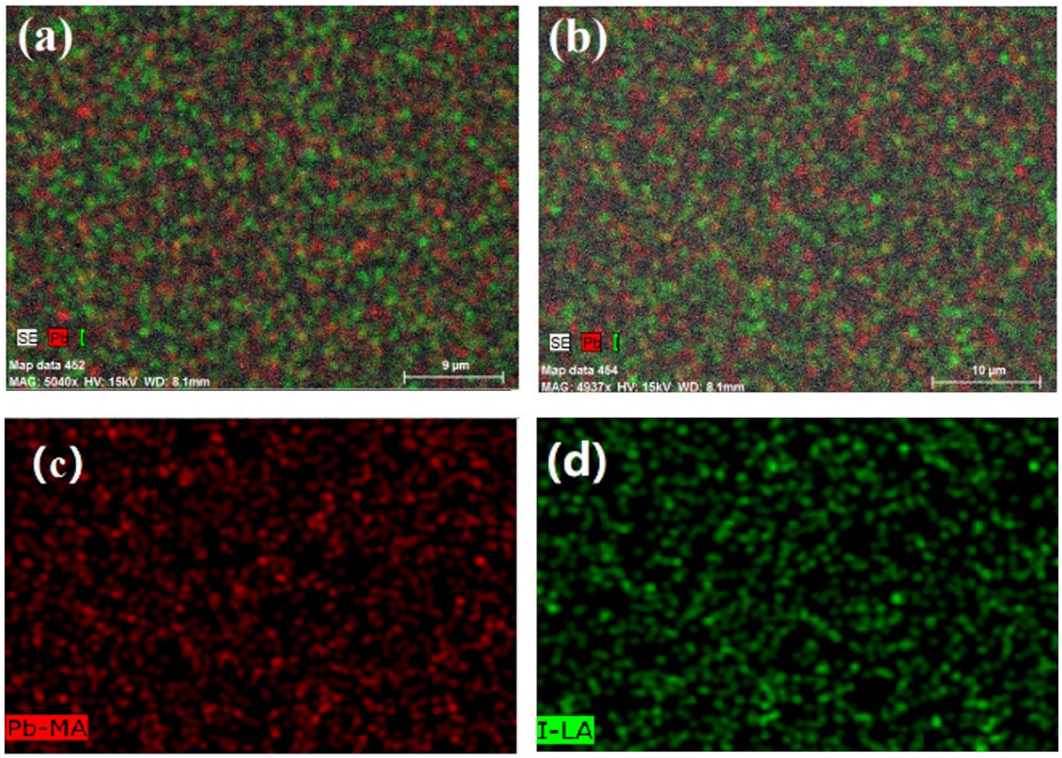

Figure 3. EDS-MAP of the $(BA)_2(MA)_3Pb_4I_{13}$ thin films (**a**) before and (**b**) after solvent annealing; distribution of (**c**) I and (**d**) Pb elements.

Sample	Pb (at%)	I (at%)	Pb/I
As-deposited films	28.21	71.79	0.392
Solvent annealed films	26.76	73.24	0.365

Table 1. Compositions of the as-deposited and solvent-annealed films determined by EDS analysis.

The composition of the $(BA)_2(MA)_3Pb_4I_{13}$ film is an important factor affecting the structural, electrical, and optical properties of the light-absorber. Figure 2 and Table 1 show the composition of the $(BA)_2(MA)_3Pb_4I_{13}$ thin films measured by EDS. Two typical peaks located at 2.48 and 3.98 keV, corresponding to the Pb and I elements. The atomic ratio of Pb to I of the as-deposited thin film is approximately 0.392. It decreases to 0.365 for the solvent annealed films, which is much close to the stoichiometry of the $(BA)_2(MA)_3Pb_4I_{13}$ film, indicating the formation of pure-phase 2D perovskite thin films. Figure 3 displays the elemental distribution of the thin film after solvent annealing, and shows that the Pb and I have uniform distribution in the entire plane without element enrichment or deficiency.

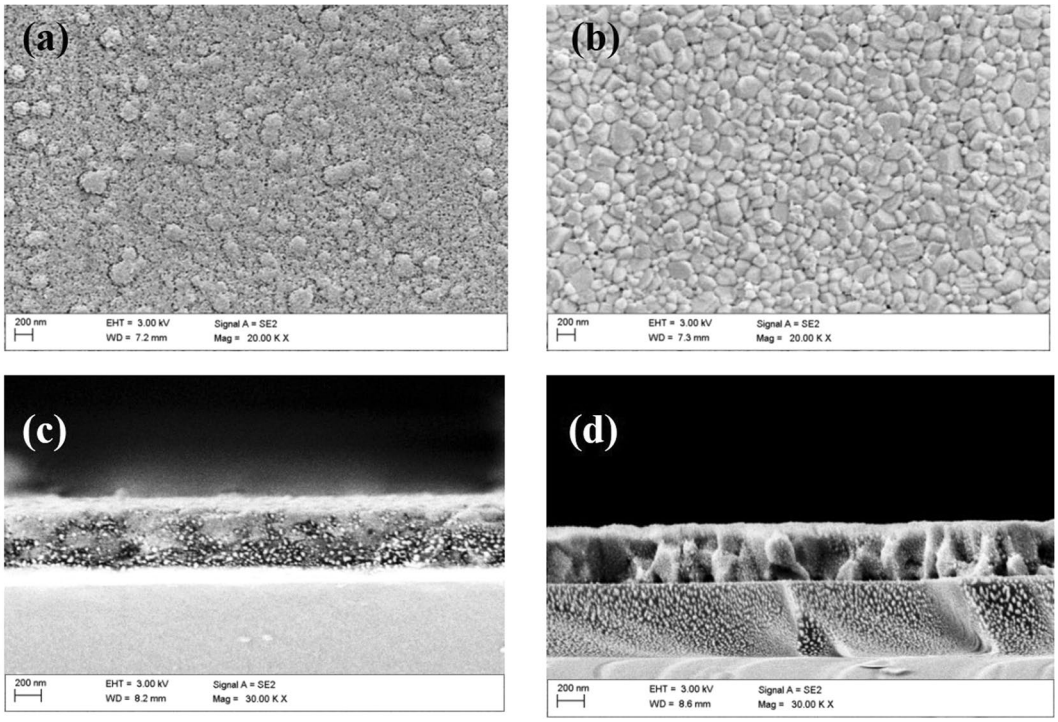

Figure 4. Morphology of the (**a**) as-deposited and (**b**) solvent-annealed film (**b**). Cross-sectional scanning electron micrographs of the (**a**) as-deposited and (**d**) solvent-annealed films.

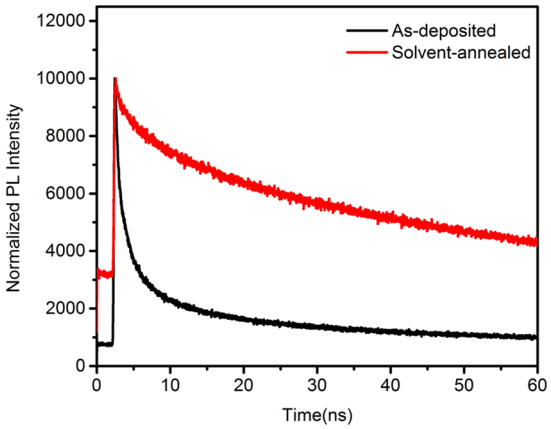

Figure 5. Time-resolved photoluminescence lifetime of the as-deposited and solvent-annealed $(BA)_2(MA)_3Pb_4I_{13}$ thin films.

Figure 4 show the morphology of as-deposited and solvent-annealed $(BA)_2(MA)_3Pb_4I_{13}$ thin films. Figure 4a illustrates that the as-deposited thin film exhibits complete surface coverage but with small grains on the substrate. The cross-section in the inset of Fig. 4a shows no distinct grains which may easily lead to poor reproducibility and photocurrent hysteresis of the 2D perovskite solar cells[30–33]. Solvent vapor of γ-butyrolactone introduced during the annealing of the 2D perovskite causes the recrystallization of $(BA)_2(MA)_3Pb_4I_{13}$. Precise control of recrystallization can improve the quality of perovskite film[34–36]. After the γ-butyrolactone vapor annealing treatment (Fig. 4b), the $(BA)_2(MA)_3Pb_4I_{13}$ thin film shows denser and larger grain distribution, and the defects are significantly reduced. Therefore, more photogenerated charges can successfully reach the electrode instead of recombining in the grain boundary.

Time-resolved PL (TRPL) decay measurements were performed to study the influence of the charge transfer process in the $(BA)_2(MA)_3Pb_4I_{13}$ thin film. Figure 5 displays the patterns and the lifetimes of the charge carriers in the thin films were estimated by fitting the data[37]. The average decay time (τ_{ave}) of the $(BA)_2(MA)_3Pb_4I_{13}$ films were calculated according to the formula, $\tau_a = (A_1\tau_1^2 + A_2\tau_2^2)/(A_1\tau_1 + A_2\tau_2)$, and the charge carrier life time extracted from the as-deposited $(BA)_2(MA)_3Pb_4I_{13}$thin films is 1.34 ns[38]. Under γ-butyrolactone solvent annealing, the TRPL lifetimes are increased to 26.29 ns, which is in very good agreement with previously reported

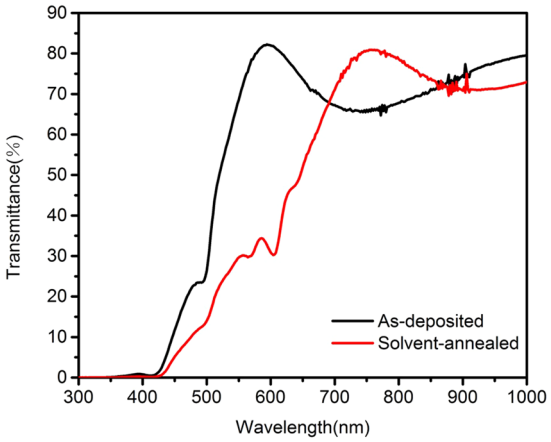

Figure 6. Optical transmittance spectra of the as-deposited and solvent-annealed $(BA)_2(MA)_3Pb_4I_{13}$ thin films.

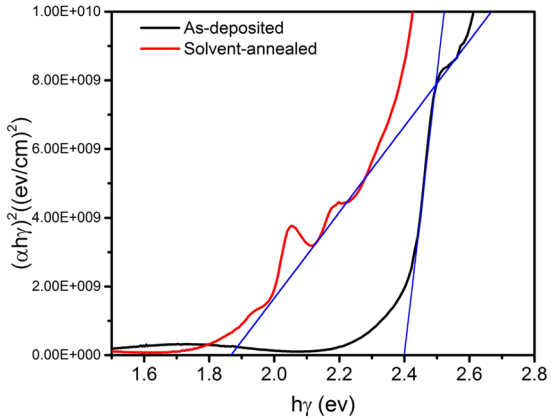

Figure 7. Estimation of the optical band gap of the as-deposited and solvent-annealed $(BA)_2(MA)_3Pb_4I_{13}$ thin films.

values[39]. Using the formula $L_D{}^2 = D\tau_s$, in which the fluorescence lifetime of perovskites and the diffusion coefficients of electrons and holes D, the electron and hole diffusion lengths are deduced to be 314 nm and 266 nm, respectively[40]. The longer lifetime (τ_s) indicates an increased charge-diffusion length (L_D) of the $(BA)_2(MA)_3Pb_4I_{13}$ thin films because of the better crystallization in the solvent-annealed thin films. This characteristic reduces the recombination of photoelectron–hole pairs.

The optical transmittance properties were obtained by a UV/visible/near-IR spectrophotometer in the wavelength range of 300–1000 nm. Figure 6 shows the transmittance spectra for the as-deposited and solvent-annealed $(BA)_2(MA)_3Pb_4I_{13}$ thin films prepared by single-source thermal evaporation. As shown in the previous SEM image, more defect states due to smaller grains, the absorption edge is clearly moving toward the IR region after solvent annealing, indicating wide range of light absorption caused by enhanced crystallinity. The absorption range of the as-deposited thin film was lower than that of the annealed thin film due to the improvement of the film's crystallinity as we mentioned above. Compared with perovskites with multiple nano-grains, the solvent-annealed perovskite film has fewer grain boundaries, this facilitates a greater range of light absorption by the absorbing layer. The band-gap energy can be calculated as $\alpha h\nu = A(h\nu - E_g)^n$, where α is the absorption coefficient, $h\nu$ is the photon energy, A is the constant, n depends on the nature of transition, and E is the band-gap energy[41]. Figure 7 shows that the band gap of the as-deposited thin film is 2.40 eV and decreases to 1.89 eV after solvent annealing, which is close to the theoretical value[42]. Hydrogen bond exists in perovskite, the presence of hydrogen bonds may affect the optical band gap of $(BA)_2(MA)_3Pb_4I_{13}$, Similarly, Filip *et al.*[43,44] have experimentally shown perovskite tunable optical bandgaps.

The perovskite solar cells with a device structure of ITO/PEDOT: PSS/2D perovskite $(BA)_2(MA)_3Pb_4I_{13}$/$PC_{61}BM$/Ag (Fig. 8a) were fabricated. PEDOT: PSS and PCBM were the hole and electron transport layers, respectively. Figure 8b shows the *J-V* curves of the $(BA)_2(MA)_3Pb_4I_{13}$ perovskite solar cells based on the as-deposited and solvent-annealed $(BA)_2(MA)_3Pb_4I_{13}$ thin film. The J_{sc}, V_{oc}, *FF*, *PCE*, R_s, and R_{sh} of the corresponding devices are summarized in Table 2. In the 2D perovskite solar cell, the $(BA)_2(MA)_3Pb_4I_{13}$ thin films without γ-butyrolactone vapor treatment are presented as the as-deposited PSCs, while the films treated with γ-butyrolactone are presented as the solvent-annealed PSCs. The as-deposited PSCs exhibit J_{sc} of 6.51 mA/cm^2,

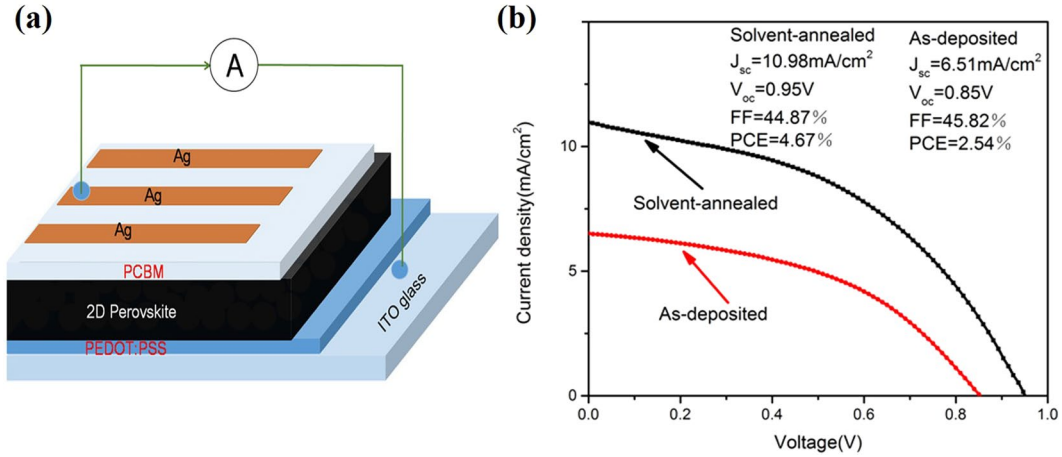

Figure 8. Device structure of (**a**) 2D perovskite solar cell; (**b**) J-V characteristics before and after solvent annealing.

Sample	V_{oc}(V)	J_{sc}(mA/cm^2)	FF	PCE	R_s(Ω)	R_{sh}(Ω)
As-deposited	0.85	6.51	45.82%	2.54%	729.93	616.78
Solvent-annealed	0.95	10.98	44.87%	4.67%	26.55	128.70

Table 2. Photovoltaic performances and fitting parameters used for the impedance spectra of the $(BA)_2(MA)_3Pb_4I_{13}$-based perovskite solar cells before and after solvent annealing.

V_{OC} of 0.85 V, *FF* of 45.82%, R_s of 729.93 Ω, and R_{sh} of 616.78 Ω. These characteristics result in a low PCE of 2.54%. Compared with the as-deposited PSCs, when the γ-butyrolactone solvent vapor is introduced during annealing, the performance of the 2D perovskite solar cell is significantly enhanced. J_{sc} substantially increases to 10.98 mA/cm^2, V_{oc} increases to 0.95 V, R_s is reduced to 26.55 Ω, and PCE increases to 4.67%. The γ-butyrolactone vapor during annealing can lead to enhanced crystallinity and larger grain size of $(BA)_2(MA)_3Pb_4I_{13}$, passivate defects, and improve device performance. Hence, the solvent annealing produces a high quality non-porous 2D perovskite film with a high purity phase, complete surface coverage, and good crystallinity. These characteristics can suppress internal recombination and leakage currents and promote photoelectric conversion of 2D perovskite solar cells.

Conclusions

The effect of solvent annealing on grain growth is investigated to enhance the photovoltaic-device efficiency of 2D perovskite $(BA)_2(MA)_3Pb_4I_{13}$ thin film prepared by single-source thermal evaporation. Solvent annealing can effectively enhance the crystallization of $(BA)_2(MA)_3Pb_4I_{13}$ thin film with denser and larger crystal grains. The element ratio of Pb/I is close to the ideal stoichiometric ratio. The films show a favorable band gap of 1.896 eV and long electron and hole diffusion lengths of 314 nm and 266 nm, respectively. The performance of the $(BA)_2(MA)_3Pb_4I_{13}$ perovskite solar cell is significantly enhanced, that is, J_{sc} remarkably increases to 10.98 mA/cm^2, V_{oc} increases to 0.95 V, and R_s is reduced to 26.55 Ω. The solvent-annealed $(BA)_2(MA)_3Pb_4I_{13}$thin-film solar cell prepared by single-source thermal evaporation shows an efficiency of 4.67%. Thus, the proposed method is promising for preparing large-area and efficient 2D perovskite solar cells.

Methods

$(BA)_2(MA)_3Pb_4I_{13}$ crystal and powder preparation. PbI_2 (7.38 g, 99.99%, Xi'an Polymer Light Technology), MAI (1.91 g, 99.5%, Xi'an Polymer Light Technology), and BAI (1.61 g, 99.5%, Xi'an Polymer Light Technology) were mixed in γ-butyrolactone (150 ml, 99%, TCI) in the beaker for 24 h with constant magnetic stirring. The 2D perovskite solution was then transferred onto a glass culture dish and maintained at 150 °C on a hot plate. Until all 2D perovskite solutions were evaporated, $(BA)_2(MA)_3Pb_4I_{13}$ crystals can be obtained as shown in Fig. 9. Then, the prepared $(BA)_2(MA)_3Pb_4I_{13}$ crystals were ground into powders as the film evaporation material.

$(BA)_2(MA)_3Pb_4I_{13}$ thin-film preparation. Figure 9 shows the fabrication of the crystals, including the $(BA)_2(MA)_3Pb_4I_{13}$ crystals preparation, single-source thermal evaporation, and solvent annealing. Prior to deposition, the ITO glass substrate was cleaned, and 0.8 g of $(BA)_2(MA)_3Pb_4I_{13}$ perovskite powder was weighed. The powder was placed in the evaporation boat. The distance from the evaporation source to the substrate was 25 cm, and the substrate speed was 40 rpm. Once the chamber pressure was pumped down to below 1×10^{-3} Pa, the working current of the evaporation source was rapidly raised to 150 A, and then the film was deposited. Until the powder was completely evaporated, the as-deposited 2D perovskite $(BA)_2(MA)_3Pb_4I_{13}$ thin films has a thickness

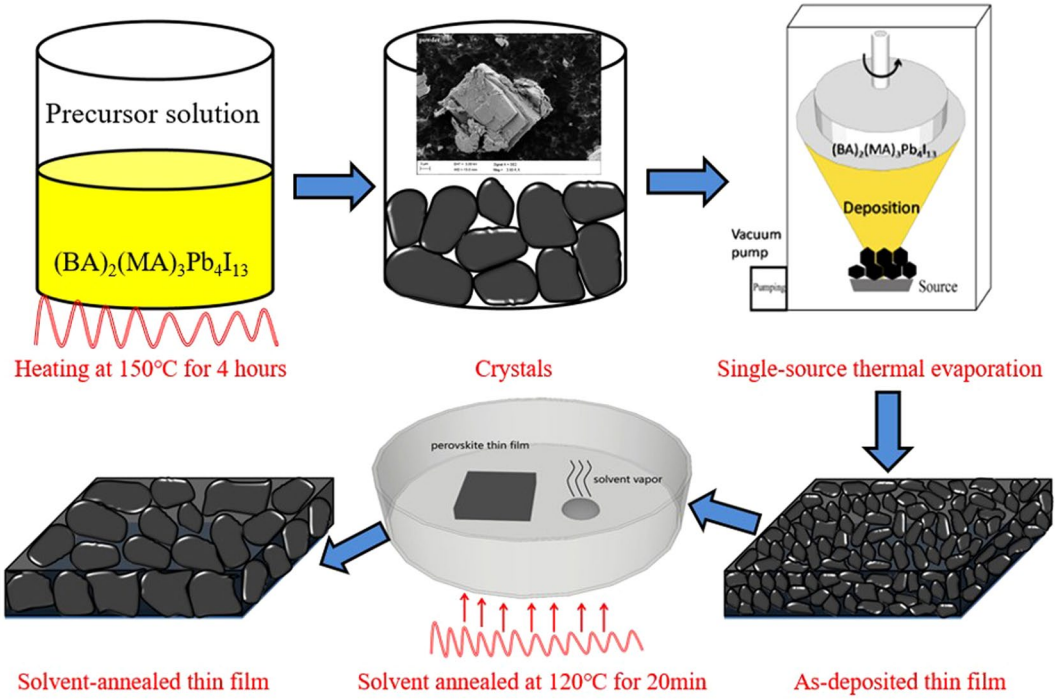

Figure 9. Schematic of the fabrication procedure including crystal preparation, single-source thermal evaporation, and solvent annealing.

of approximately 400 nm. Solvent annealing was then performed under a γ-butyrolactone atmosphere (40 μl) at 120 °C for 20 min.

Device fabrication. The perovskite solar cells have a device structure of ITO/PEDOT: PSS/$(BA)_2(MA)_3Pb_4I_{13}$/$PC_{61}BM$/Ag was prepared. An aqueous solution of PEDOT-PSS (CLEVIOS PVP AI4083) was spin-coated onto ITO glass substrate to form a 50-nm thick thin film (4500 rpm for 40 s). The obtained PEDOT-PSS film was placed on a hot plate at 160 °C for 20 minutes and then transferred to a single source evaporation deposition system. The $(BA)_2(MA)_3Pb_4I_{13}$ absorber layer was deposited by single-source thermal evaporation and then solvent annealed in a N_2-filled glove-box for 20 min at 120 °C. The $PC_{61}BM$ solution (20 mg/ml in chlorobenzene) was spin-coated on the $(BA)_2(MA)_3Pb_4I_{13}$ thin film at 3000 rpm for 30 s. Lastly, 90 nm-thick Ag cathode was prepared by thermal evaporation in a vacuum of approximately 3.0×10^{-4} Pa.

Characterization. The crystalline structure of the $(BA)_2(MA)_3Pb_4I_{13}$ thin films and powder were analyzed by X-ray diffractometer (Ultima IV). The composition and surface morphology of perovskite film and powder were analyzed by energy-dispersive X-ray microanalysis system (Bruker QUANTAX 200, Bruker, Billerica, MA, USA) and a SUPRA 55 scanning electron microscope, respectively. The time-resolved PL was recorded using the steady-state spectroscopy and time-resolved (Fluo Time 300, Pico Quant GmbH). The thickness of the $(BA)_2(MA)_3Pb_4I_{13}$ thin films were measured by a DEKTAK XT profilometer (Bruker, Billerica, M A, USA). The optical transmittance properties were obtained by a UV/visible/near-IR spectrophotometer (Lambda 950, PerkinElmer). The *J-V* curves of the 2D perovskite solar cells were recorded in simulated AM 1.5 G conditions (100 mW/cm^2) with a Keithley 2400 Source Measure Unit.

Data availability

All data included in this study are available upon request by contact with the corresponding author.

Received: 26 May 2019; Accepted: 4 November 2019;
Published online: 22 November 2019

References

1. Liang, G. X. *et al*. Enhanced Crystallinity and Performance of $CH_3NH_3PbI_3$ Thin Film Prepared by Controlling Hot CH_3NH_3I Solution Onto Evaporated PbI_2 Nanocrystal. *IEEE journal of photovoltaic.* **6**, 1537–1541 (2016).
2. Shi, D. *et al*. Solar cells. *Low trap-state density and long carrier diffusion in organolead trihalide perovskite single crystals, Science.* **347**, 519–522 (2015).
3. Pisoni, S. *et al*. Tailored lead iodide growth for efficient flexible perovskite solar cells and thin-film tandem devices, NPG Asia. *Materials* **10**, 1076–1085 (2018).
4. NREL Efficiency chart, https://www.nrel.gov/pv/cell-efficiency. html, access on April 17 2019.
5. Sahli, F. *et al*. Fully textured monolithic perovskite/silicon tandem solar cells with 25.2% power conversion efficiency. *Nature Materials.* **17**, 820–826 (2018).
6. Yang, W. S. *et al*. Iodide management informamidinium lead-halide–based perovskite layers for efficient solar cells. *Science.* **356**, 1376–1379 (2017).

7. Liu, C. *et al*. Efficiency and stability enhancement of perovskite solar cells by introducing $CsPbI_3$ quantum dots as an interface engineering layer, NPG Asia. *Materials* **10**, 552–561 (2018).
8. Ke, Wj *et al*. Compositional and Solvent Engineering in Dion–Jacobson 2D Perovskites Boosts Solar Cell Efficiency and Stability. *Adv. Energy Mater.* **9**, 1803384 (2019).
9. Sun, X. *et al*. Mixed-solvent-vapor annealing of perovskite for photovoltaic device efficiency enhancement. *Nano Energy* **28**, 417–425 (2016).
10. Cao, D. H., Stoumpos, C. C., Farha, O. K., Hupp, J. T. & Kanatzidis, M. G. 2D homologous perovskites as light-absorbing materials for solar cell applications. *J. Am. Chem. Soc.* **137**, 7843–7850 (2015).
11. Wei, Y. *et al*. Reverse-Graded 2D Ruddlesden–Popper Perovskites for Efficient Air-Stable Solar Cells. *Adv. Energy Mater*. 1900612 (2019).
12. Cortecchia, D. *et al*. Lead-free $MA_2CuCl_xBr_{4-x}$ hybrid perovskites. *Inorg. Chem.* **55**, 1044–1052 (2016).
13. Xiao, Z. *et al*. Photovoltaic properties of two-dimensional$(CH_3NH_3)_2Pb(SCN)_2I_2$ perovskite: a combined experimental and density-functional theory study. *J. Phys. Chem. L.* **7**, 1213–1218 (2016).
14. Zhang, X. *et al*. Phase Transition Control for High Performance Ruddlesden–Popper Perovskite Solar Cells. *Adv. Mater.* **30**, 1707166 (2018).
15. Im, J. H., Chung, J., Kim, S. J. & Park, N. G. Synthesis, structure, and photovoltaic property of a nanocrystalline 2H perovskite-type novel sensitizer $(CH_3CH_2NH_3)PbI_3$. *Nanoscale Res. Lett.* **7**, 1–7 (2016).
16. Zhang, J. J. *et al*. Binary Solvent Engineering for high-performance two-dimensional perovskite Solar Cells. *ACS Sustainable Chem. Eng.* **7**, 3487–3495 (2019).
17. Gan, X. Y. *et al*. 2D homologous organic-inorganic hybrids as light-absorbers for planer and nanorod-based perovskite solar cells. *Solar Energy Materials & Solar Cells* **162**, 93–102 (2017).
18. Lin, Y. *et al*. Enhanced Thermal Stability in Perovskite Solar Cells by Assembling 2D/3D Stacking Structures. *J. Phys. Chem. Lett.* **9**, 654–658 (2018).
19. Fan, P. *et al*. High-performance perovskite $CH_3NH_3PbI_3$ thin films for solar cells prepared by singlesource physical vapour deposition. *Sci. Rep.* **6**, 29910 (2016).
20. Chen, C. Y. *et al*. All-Vacuum-Deposited Stoichiometrically Balanced Inorganic Cesium Lead Halide Perovskite Solar Cells with Stabilized Efficiency Exceeding 11%. *Adv. Mater.* **29**, 1605290 (2017).
21. Liu, J. *et al*. Improved Crystallization of Perovskite Films by Optimized Solvent Annealing for High Efficiency Solar Cell. *ACS Appl. Mater. Interfaces* **7**, 24008–24015 (2015).
22. Fan, P. *et al*. Hysteresis-free two-dimensional perovskite solar cells prepared by singlesource physical vapour deposition. *Solar Energy* **169**, 179–186 (2018).
23. Liang, G. X. *et al*. Highly Uniform Large-Area (100 cm^2) Perovskite $CH_3NH_3PbI_3$ Thin-Films Prepared by Single-Source Thermal Evaporation. *Coatings* **8**, 256 (2018).
24. Xiao, Z. *et al*. Giant switchable photovoltaic eect in organometal trihalide perovskite devices. *Adv. Mater.* **26**, 6503–6509 (2015).
25. Liu, C. *et al*. Efficient Perovskite Hybrid Photovoltaics via Alcohol-Vapor Annealing Treatment. *Adv. Funct. Mater.* **26**, 101–110 (2015).
26. Zhang, F. *et al*. sec-Butyl alcohol assisted pinhole-free perovskite film growth for high-performance solar cells. *J. Mater. Chem. A*. **4**, 3438–3445 (2016).
27. Gangadharan, D. T. *et al*. Aromatic Alkylammonium Spacer Cations for Efficient Two-Dimensional Perovskite Solar Cells with Enhanced Moisture and Thermal Stability. *Sol. RRL* **2**, 1700215 (2018).
28. Peng, H. X. *et al*. High-Quality Perovskite $CH_3NH_3PbI_3$ Thin Films for Solar Cells Prepared by Single-Source Thermal Evaporation Combined with Solvent Treatment. *Materials*. **12**, 1237 (2019).
29. Jeon, N. J. *et al*. Compositional engineering of perovskite materials for high-performance solar cells. *Nature*. **517**, 476–480 (2015).
30. Liu, B. *et al*. Optical Properties and Modeling of 2D Perovskite Solar Cells. *Sol. RRL*. **1**, 1700062 (2017).
31. Zhang, X. *et al*. Stable high efficiency two-dimensional perovskite solar cells via cesium doping. *Energy Environ. Sci.* **10**, 2095–2102 (2017).
32. Stoumpos, C. C. *et al*. High Members of the 2D Ruddlesden-Popper Halide Perovskites: Synthesis, Optical Properties, and Solar Cells of $(CH_3(CH_2)_3NH_3)_2(CH_3NH_3)_4Pb_5I_{16}$. *Chem*. **2**, 427–440 (2017).
33. Park, N. G. Crystal growth engineering for high efficiency perovskite solar cells. *CrystEng Comm.* **18**, 5977–5985 (2016).
34. Chen, J. L. *et al*. Doped tin induced structural evaluation and performance of $CH_3NH_3Pb_xSn_{1-x}I_3$ thin films prepared by a simple route of unisource thermal evaporation. *J Mater Sci: Mater Electron.* **27**, 13192–13198 (2016).
35. Zhang, X. Q. *et al*. Vertically Oriented 2D Layered Perovskite Solar Cells with Enhanced Efficiency and Good Stability. *small* **13**, 1700611 (2017).
36. Zhou, N. *et al*. Exploration of Crystallization Kinetics in Quasi Two-Dimensional Perovskite and High Performance Solar Cells. *J. Am. Chem. Soc.* **140**, 459–465 (2018).
37. Reynolds, D. C. *et al*. Time-resolved photoluminescence lifetime measurements of the Γ5 andΓΓ6 free excitons in ZnO. *J. Appl. Phys.* **88**, 2152 (2000).
38. Wang, J. *et al*. Purcell effect in an organic-inorganic halide perovskite semiconductor microcavity system. *Appl. Phys. Lett*. **108**, 022103 (2016).
39. Chen, Y. *et al*. Tailoring Organic Cation of 2D Air-Stable Organometal Halide Perovskites for Highly Efficient Planar Solar Cells. *Adv. Energy Mater.* **7**, 1700162 (2017).
40. Muller, J. *et al*. Composition, structure and optical properties of sputtered thin films of $CuInSe_2$. *Thin Solid Films*. **496**, 364–370 (2006).
41. Peng, H. X. *et al*. vapor effect on microstructural and optical properties of $CH_3NH_3PbI_3$ film during solvent annealing. *Surface & Coatings Technology* **359**, 162–168 (2019).
42. Stoumpos, C. C. *et al*. Ruddlesden-Popper Hybrid Lead Iodide Perovskite 2D Homologous Semiconductors. *Chem. Mater.* **28**, 2852–2867 (2016).
43. Lee, J. H., Lee, J. H., Kong, E. H. & Jang, H. M. The nature of hydrogen-bonding interaction in the prototypic hybrid halide perovskite, tetragonal $CH_3NH_3PbI_3$. *Scientific Reports* **6**, 21687 (2016).
44. Filip, M. R., Eperon, G. E., Snaith, H. J. & Giustino, F. Steric engineering of metal halide perovskites with tunable optical band gaps. *Nat. Commun.* **5**, 5757 (2014).

Acknowledgements

Zheng and Lan contributed equally. This work was supported by National Key R&D Program of China (No. SQ2018YFE020412), The Key Project of Department of Education of Guangdong Province (No. 2018KZDXM059), National Natural Science Foundation of China (Grant No. 61404086), Shenzhen Key Lab Fund (ZDSYS 20170228105421966), Basic Research Program of Shenzhen (JCYJ20180305124340951).

Author contributions

Liang and Fan designed and conducted the project. Zheng, Lan, and Su conducted the experiments. Data analyses were performed by Zheng, Lan, Su, Peng, and Luo. This manuscript was written by Lan. All authors reviewed this manuscript.

Competing interests

The authors declare no competing interests.

Additional information

Correspondence and requests for materials should be addressed to G.-X.L.

Reprints and permissions information is available at www.nature.com/reprints.

Publisher's note Springer Nature remains neutral with regard to jurisdictional claims in published maps and institutional affiliations.